Electronic Supplementary Material (ESI) for Energy & Environmental Science.

Supporting Information

Green mechanochemical Li foil surface reconstruction toward long-life Li-metal pouch cells

Kecheng Long[a], Shaozhen Huang[a], Han Wang[c], Anbang Wang[b], Yuejiao Chen[a], Zhijian Liu[a], Yu Zhang[c], Zhibin Wu[a], Weikun Wang[b, *] and Libao Chen[a, *]

[a] State Key Laboratory of Powder Metallurgy, Central South University, Changsha, Hunan 410083, China

[b] Research Institute of Chemical Defense, Beijing 100191, China

[c] Beihang University, Beijing 100191, China

*Corresponding author. E-mail: wangweikun2022@163.com, lbchen@csu.edu.cn

Experimental Section

1. Materials

Fumed silica with a specific surface area of 200 m^2/g was purchased by Shanghai Aladdin Biochemical Technology Co., Ltd. (China). Commercail Li foil with the thickness of 120 μm and 160 μm were purchased by Tianjin Zhongneng Lithium Industry Co., Ltd. (China). The $LiFePO_4$ (LFP) powder and commercial LCO cathode electrodes were provided by Dongguan Juda Electronics Co., Ltd. (China).

2. Fabrication of PRS@Li and ERS@Li

The schematic of the process of mechanochemical Li foil surface reconstruction was shown in Fig. 1d. For fabrication of PRS@Li, in the drying room with dew point below -40 ℃, the appropriate amount of fumed silica powder (≈ 4.5 mg) was gently and evenly smeared on the Li foil surface (8 cm × 5 cm) without strongly friction. The ERS@Li was prepared by strongly rubbing the surface of PRS@Li to make is black. Finally, excess fumed silica powder was then removed from the surface of Li foil and the load of modified layer is about 0.088 mg/cm^2.

3. Material Characterization

A normal scanning electron microscope (SEM, JEOL JSM-7610FPlus equipped with an Oxford ULTIM MAX 40 energy spectrometer) and a vacuum transfer accessory were conducted at KW-ST Lab (www.kewei-scitech.com) was used to visualize the micromorphology. High-resolution transmission electron microscopy (HR-TEM) and selected domain electron diffraction (SAED) of the fumed silica nanoparticles were taken with a transmission electron microscope (TEM, JEOL JEM-F200 equipped with a jed2300 energy spectrometer). The surface chemical composition of the Li metal anode and fumed silica were analyzed by X-ray photoelectron spectroscopy (XPS, Thermo Scientific K-Alpha+), which equipped with a vacuum transfer accessory were conducted at KW-ST Lab (www.kewei-scitech.com). Seal the Li electrode with its surface soaked in electrolyte in a quartz tube, and then conduct Raman testing at the Li/electrolyte interface. (Raman, Nicolet Is50, Thermo Fisher Scientific). The contact

angles of liquid electrolytes (10 μL droplets) on the surface of the Li electrodes were measured at 25 ℃ on a Contact Angle System OCA 20 (Dataphysics, Germany) in a drying room.

4. Electrochemical Measurements

To investigate the electrochemical behavior of the Li electrodes, the Li||Li symmetrical cells, Li||LFP button full cells, 0.53 Ah Li||$LiCoO_2$ (LCO) pouch cells, 1.6 Ah Li||S pouch cells and 6.4 Ah Li||S pouch cells were assembled. The discharge or charge measurements were conducted on a Neware battery test system or a Land battery test system. Li||Li symmetrical cells and Li||LFP button full cells were assembled by CR2016 button cell, using Celgard 2400 as the separator. 0.12 mm-thin Li electodes with a diameter of 14.0 mm were employed as the anode materials. For Li||Li symmetrical cells, using 45 μL 1 M $LiN(CF_3SO_2)_2$ (LiTFSI) in DOL/DME (V/V = 1/1) with 2 wt% $LiNO_3$ additive. For Li||LFP button full cells, using 45 μL 1.0 M LiPF6 in ethylene carbonate (EC)/ethyl methyl carbonate (EMC)/fluoroethylene carbonate (FEC) (V/V/V = 3:7:1) as the electrolyte. The cathode of Li||LFP button full cells was prepared by casting LFP slurry into an aluminum foil. The slurry consisted of commercial LFP powder, carbon black, and polyvinylidene fluoride (PVDF) binder (8:1:1 by mass) in N-methyl-2-pyrrolidone (NMP) and the active substance mass was controlled at 12-13 mg/cm^2. The pouch cells were assembled in a drying room. Using a turn stacking process, the 1.6 Ah Li||S pouch cells were assembled by a 160 μm-thin lithium foil with a width of 8 cm and a length of 28 cm, four pieces of double coated sulfur cathode electrodes with a size of 5 cm × 7.5 cm and a piece of 15 μm-thin PE separator (8.3 cm × 56 cm). The sulfur cathodes were prepared as described in our previous papers [1]. The design parameters of the 1.6 Ah Li||S pouch cell were shown in Table S3. The 6.4 Ah Li||S pouch cells were obtained by a lamination process, which stacked by 8 pieces of double coated sulfur cathode electrodes with a size of 9.6 cm × 6.8 cm, 9 pieces of 100 μm-thin lithium metal anode electrode with a size of 9.9 cm × 7.1 cm and 9 μm-thin PE separator. Using a ether-based liquid electrolyte (0.6 M $LiN(CF_3SO_2)_2$ (LiTFSI) in DOL/DME (V/V = 1/1) with 0.4 M $LiNO_3$ additive) as the

electrolyte of Li||S pouch cells and the E/S weight ratio is 3.2 $g_{electrolyte}/g_{sulfur}$. The 0.53 Ah Li||LCO pouch cells were obtained by a lamination process, which stacked by three pieces of commercial LCO cathode electrodes (areal LCO loading of ~ 35 mg/cm^2 (double-sided)) with a size of 4.7 cm × 7.7 cm, four pieces of 120 μm-thin lithium metal anode electrode with a size of 5 cm × 8 cm and a piece of 15 μm-thin PE separator (8.3 cm × 45 cm). Using a local high concentration electrolyte (1.5 M LiFSI in DME/1,1,2,2-Tetrafluoroethyl-2,2,3,3-tetrafluoropropylether (TTE) (1.2:3 by mole)) as the electrolyte for Li||LCO pouch cells. The pouch cells were rested for 1 day before electrochemical tests. The Li||S pouch cells were galvanostatically discharged to 1.8 V at 0.2 C and charged to 2.6 V at 0.1 C for cycle test (1 C = 1000 mAh/g) and the Li||LCO pouch cells were galvanostatically discharged to 3 V at 0.5 C and charge to 4.2 V at 0.3 C for cycle test (1C = 145 mAh/g). Electrochemical impedance spectroscopy (EIS) was performed in the frequency range of 100 KHz to 0.1 Hz with an alternating voltage amplitude of 5 mV. The Tafel curves of Li||Li symmetrical cells were measured at a scan rate of 1 mV/s from -0.15 to 0.15 V. The exchange current density was calculated based on Tafel equation. Chronoamperometry (CA) test of Li||Li symmetric cells were measured at the constant voltage of 150 mV for 30 min. The EIS, Tafel curves and chronoamperometry (CA) were recorded on electrochemical workstation (Princeton PARSTAT 4000, AMETEK Co. Ltd).

5. COMSOL Multiphysics Simulation

Finite element modeling was conducted using COMSOL Multiphysics software. The current in electrolytes and electrodes were simulated by using the tertiary current distribution model interface. The electrolyte current is solved according to Ohm's law. One electrode is grounded, and the other is set to the battery potential to meet the total current condition. The electrode dynamics that occur at the interface of Li metal electrode is described by the Butler-Volmer equation. The initial value of the electrolyte potential is set to be equivalent to the battery potential at open circuit (i.e., when the potential is not activated). The transport of dissolved ions generated by electrode reactions in the electrolyte is modeled through transient simulation of the "dilute

material transport" interface, assuming that ion transport can be described by diffusion according to Fick's law. In the third current density distribution, the Nernst-Planck equation is used in the mass transfer simulation, and the mass transfer caused by diffusion and migration is also considered. According to the distribution of the electrochemical reaction active sites of Li foil electrode, PRS@Li electrode and ERS@Li electrode (Fig. 2 and Fig. S4), the corresponding models are shown in the Fig. S5. A square region with a size of 500 × 500 nm^2 was established as study area and the current density was set to 2.5 mA cm^{-2}. The initial Li^+ concentration in the electrolyte is 1M. Due to the mixing of lithiated fumed silica and metal, the conductivity of lithiated fumed silica nanoparticles on Li surface is the same as that of metal lithium, which is 1.26 × 10^7 S/m. The diffusion coefficients of Li^+ in bulk electrolyte was assumed to be 1 × 10^{-9} m^2/s.

6. Density functional theory (DFT) calculations

Density functional theory as implemented in the Vienna Ab-initio Simulation Package (VASP) was employed to optimize geometry structures.[2, 3] The exchange-correlation interactions were described by the generalised gradient approximation (GGA)[4] in the form of the Perdew-Burke-Ernzerhof functional (PBE)[5]. A cut-off energy of 500 eV for plain-wave basis sets was adopted and the convergence threshold was 10^{-5} eV, and 5×10^{-3} eV/Å for energy and force, respectively. The weak interaction was described by DFT+D3 method using empirical correction in Grimme's scheme.[6] The vacuum space was set to be more than 20 Å, which was enough to avoid the interaction between periodical images. For Li_2CO_3, Li_2SiO_3, Li_4SiO_4, LiOH, and SiO_2, (001) surface was calculated, and the (111) surface was used for Li_2O.

The adsorption energy of FSI^- and $TSFI^-$ adsorbed on the surface of those materials can be calculated by the following equation;

$$\Delta E = E(total) - E(surface) - E(molecule)$$

Where E(total) is the total energy with small molecule adsorbed on surface, E(surface) and E (molecule) refer to the calculated energy for surface and small molecule,

respectively.

7. MD calculations

Determine force field parameters. Quantum chemistry calculations were first performed to optimize molecular geometries of anions and solvent molecules using the Gaussian 16 package[7] at B3LYP/6-311+G(d) level of theory. The atomic partial charges on these solvent molecules were computed by fitting to the molecular electrostatic potential at atomic centers with the Møller-Plesset second-order perturbation method and the correlation-consistent polarized valence cc-pVTZ(-f) basis set. The atomistic force field parameters for all ions and molecules are described by the AMBER format and are taken from previous work.[8] The cross-interaction parameters between different atom types are obtained from the Lorentz-Berthelot combination rule.

Molecular Dynamics Pretreatment of Electrolyte. A bulk modelling system consisting of 125 LiTFSI ion pairs, 600 DME molecules and 894 DOL molecules was constructed. Atomistic simulations were performed using GROMACS package with cubic periodic boundary conditions.[9] The equations for the motion of all atoms were integrated using a classic Verlet leapfrog integration algorithm with a time step of 1.0 fs. A cutoff radius of 1.6 nm was set for short-range van der Waals interactions and real-space electrostatic interactions. The particle-mesh Ewald (PME) summation method with an interpolation order of 5 and a Fourier grid spacing of 0.15 nm was employed to handle long range electrostatic interactions in reciprocal space. All simulation systems were first energetically minimized using a steepest descent algorithm, and thereafter annealed gradually from 700 K to room temperature (300 K) within 10 ns. All annealed simulation systems were equilibrated in an isothermal-isobaric (NPT) ensemble for 10 ns of physical time maintained using a Nosé-Hoover thermostat and a Parrinello-Rahman barostat with time coupling constants of 0.4 and 0.2 ps, respectively, to control the temperature at 300 K and the pressure at 1 atm.

Model construction and simulation methods. A surface layer of Li electrode consisting of 150 Li_2O, 150 LiOH, and 150 Li_2CO_3 was constructed. An additional surface layer of Li electrode consisting of 60 Li_2O, 60 LiOH, 60 Li_2CO_3, 60 SiO_2, 60

Li_2SiO_3 and 60 Li_4SiO_4 was also constructed. These two surface layer materials were equilibrated leading to thick film with a dimension of 5.0 nm * 5.0nm and a thickness of approximately 1.0 nm.

The bulk electrolyte system was then position above the constructed two surface layer, respective, to construct two modelling systems. These two complex systems were further confined between two Li electrodes with Li (110) in contact with bulk electrolytes and the constructed surface layer. Each Li (110) electrode consists of three Li layers and is composed of 1224 Li atoms.

The constructed surface layer and Li (110) electrodes were positioned parallel to the XY plane of an externally defined Cartesian coordination system. The distance between Li electrodes facing the confined solvent electrolytes in the anode and cathode is set to ~9.0 nm along the Z axis to ensure that solvent molecules and ions adopts bulk-like behavior in the central portion of the confined environment. The periodic distance of this Cartesian coordination system on the Z axis is 16.0 nm, which is sufficiently large such that interactions between the confined solvent molecules and electrolyte ions and the periodic image of the Li electrodes in the top plane can be eliminated. For charging the modelling systems, a simplified and efficient approach was employed by assigning quantitative partial charges to top atoms in Li (110) electrodes that are in direct contact with the confined solvent electrolytes.[10] The anode and cathode are allocated with positive and negative partial charges, respectively, with the potential between two electrodes of 0.2V. The atomistic force field parameters for all ions and molecules are described by the AMBER format and are taken from previous work.[8] The cross-interaction parameters between different atom types are obtained from the Lorentz-Berthelot combination rule.

The complex modelling system was again energetically minimized using a steepest descent algorithm, and thereafter annealed gradually from 700 K to room temperature (300 K) within 10 ns using above mentioned simulation parameters. The annealed simulation system was equilibrated in an NVT ensemble for 10 ns of physical time maintained using a Nosé-Hoover thermostat and a Parrinello-Rahman barostat with time coupling constants of 0.4 and 0.2 ps, respectively, to control the temperature

at 300 K. Atomistic simulations were further performed in a canonical ensemble (NVT) for 50 ns, and simulation trajectories were recorded at an interval of 100 fs for further structural and dynamical analysis.

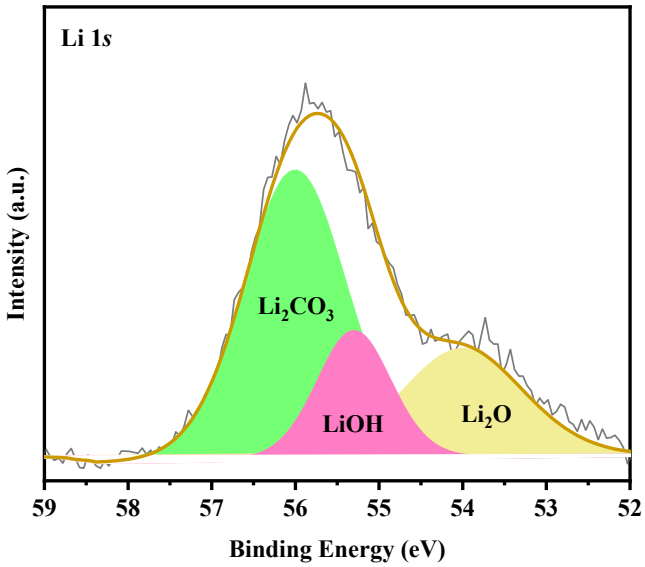

Fig. S1 The Li 1*s* spectrums of the surface of Li foil.

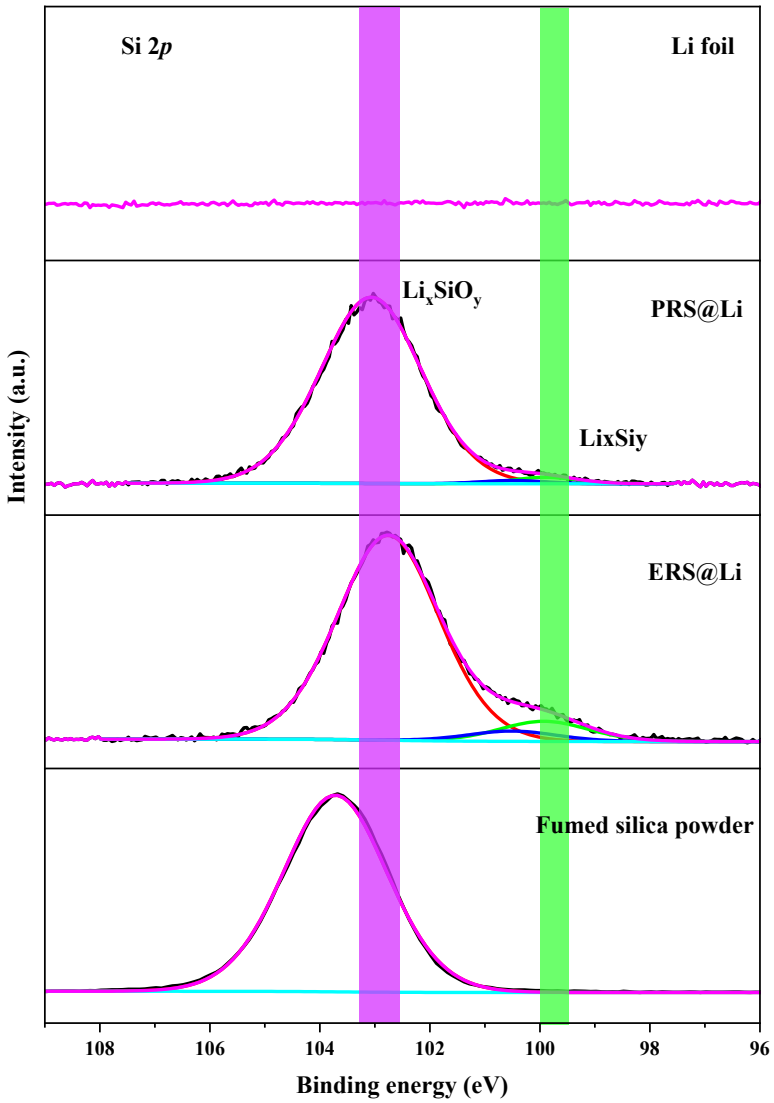

Fig. S2 Si 2*p* spectrums of the surface of Li foil, PRS@Li, ERS@Li and fumed silica powder.

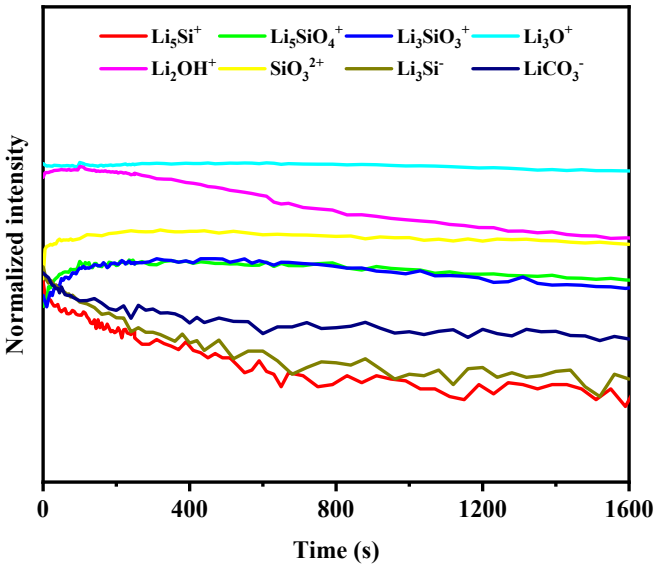

Fig. S3 The curve of normalized intensity of charged ions changing with etching time for ERS@Li.

The ERS layer mainly consists of Li_2O, Li_2CO_3, LiOH, Li_4SiO_4, Li_2SiO_3, Li_xSi_y and unreacted SiO_2. Among them, Li_4SiO_4, Li_2SiO_3, and Li_xSi_y originate from the mechanochemical reaction between SiO_2 and Li. Due to the greater impact of mechanical friction on the upper surface, the thorough reaction product (Li_xSi_y) of Li and silica is more distributed on the upper surface.

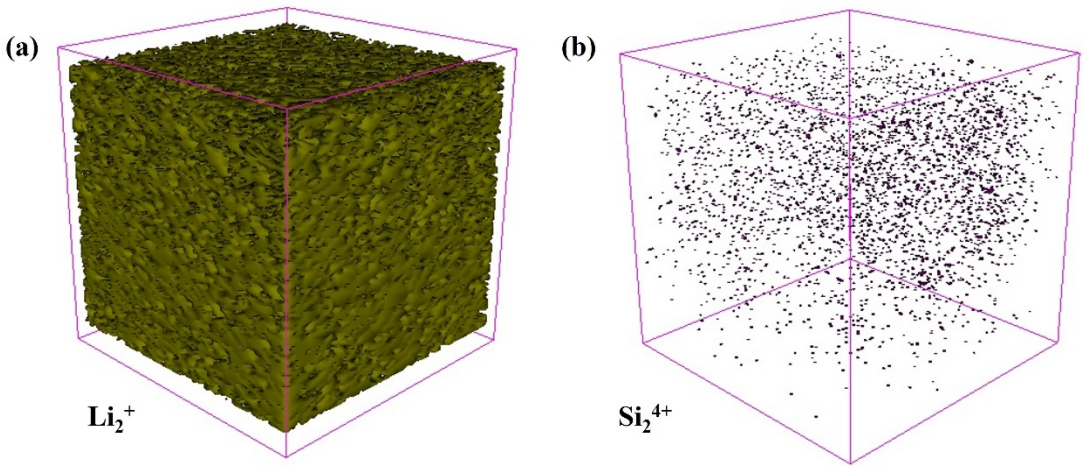

Fig. S4 3D structure views of **a** Li_2^+ positive ions and **b** Si_2^{4+} positive ions for TOF-SIMS depth sputtering on the surface of ERS@Li.

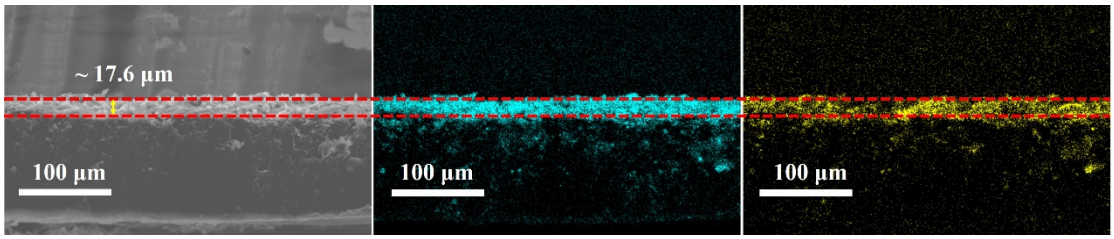

Fig. S5 Side-view SEM image of ERS@Li.

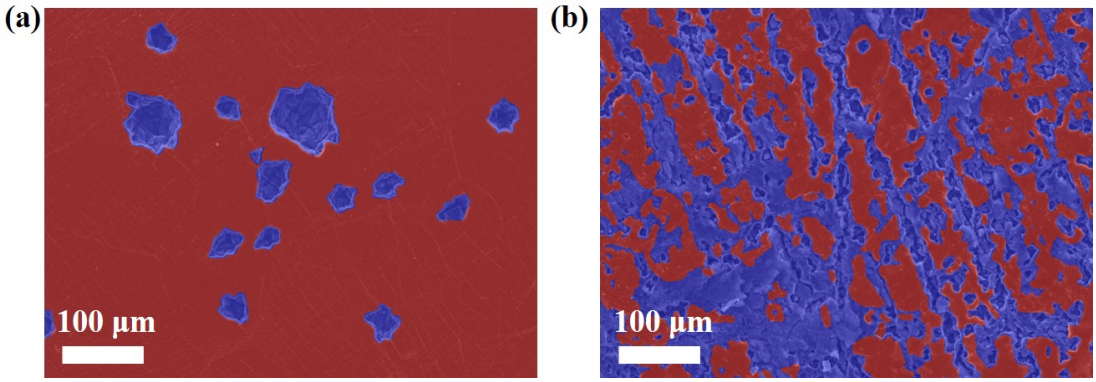

Fig. S6 The surface morphology of **a** Li foil and **b** PRS@Li after CA test. The blue represents active region and the red represents inactive region. The active region area of Li foil electrode is 8% and PRS@Li electrode is 56%.

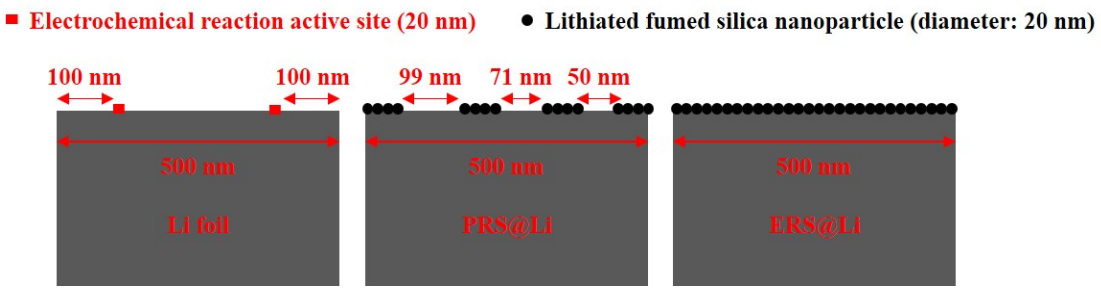

Fig. S7 The interface model of Li foil electrode, PRS@Li electrode and ERS@Li electrode for finite element simulation.

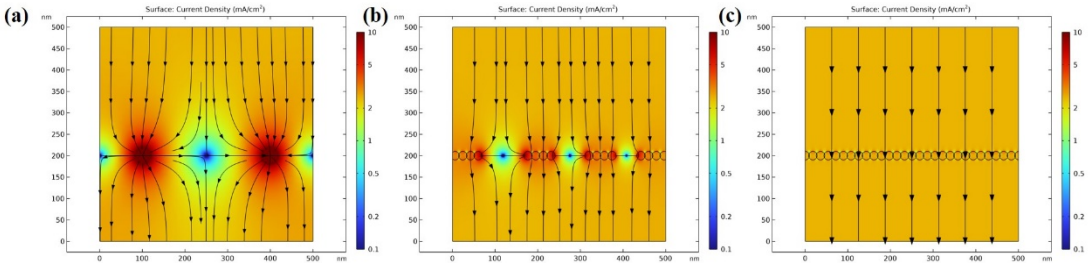

Fig. S8 The current density distribution of **a** Li foil, **b** PRS@Li and **c** ERS@Li at the electrochemical interface by finite element method simulation.

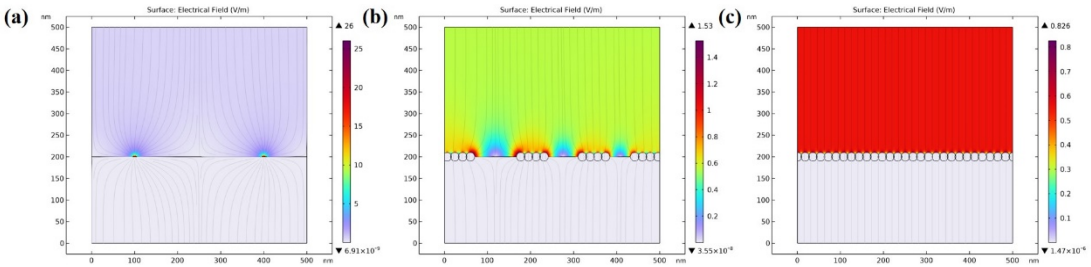

Fig. S9 The electric field distribution of **a** Li foil, **b** PRS@Li and **c** ERS@Li at the electrochemical interface by finite element method simulation.

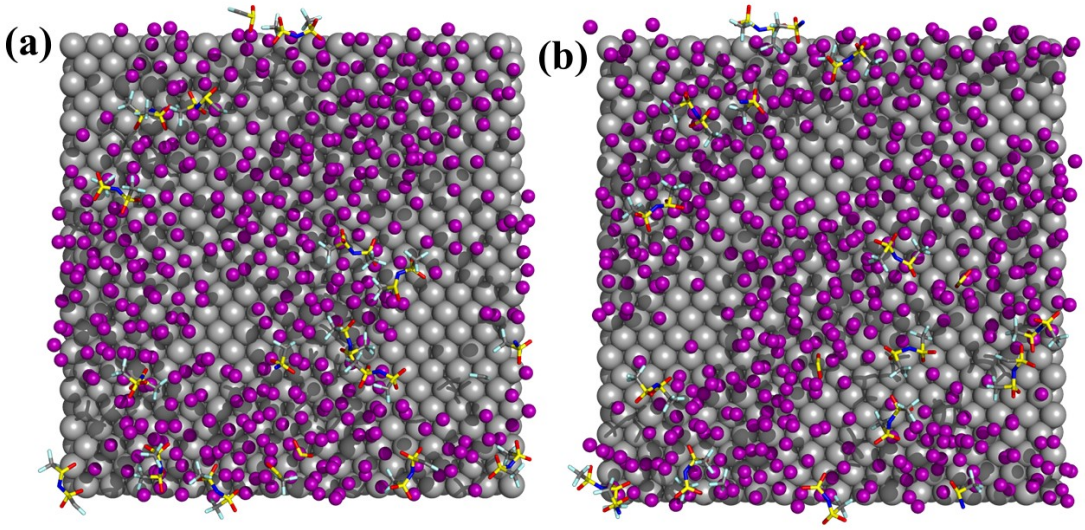

Fig. S10 The distribution of Li^+-($TFSI^-$) near **a** primitive surface of Li foil and **b** reconstructed surface.

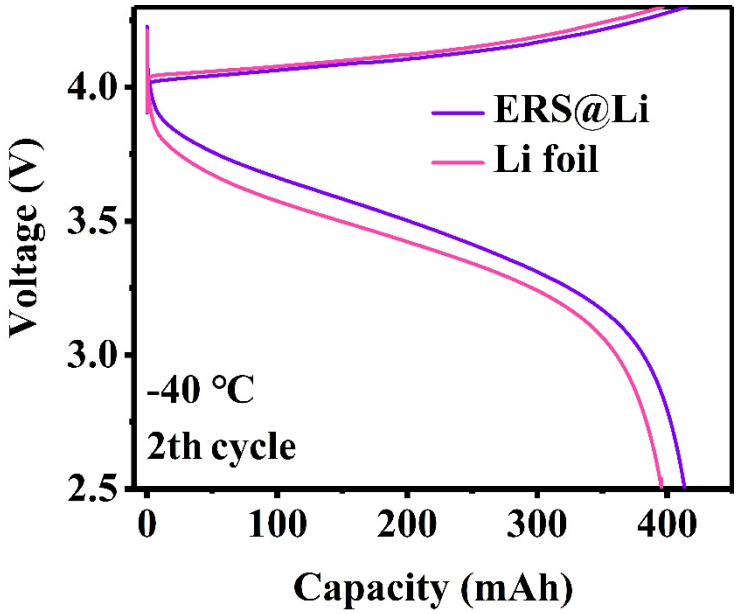

Fig. S11 The 2th charge-discharge curves of Li||LCO pouch cells at -40 ℃ at 0.01 C charge and 0.05 C discharge.

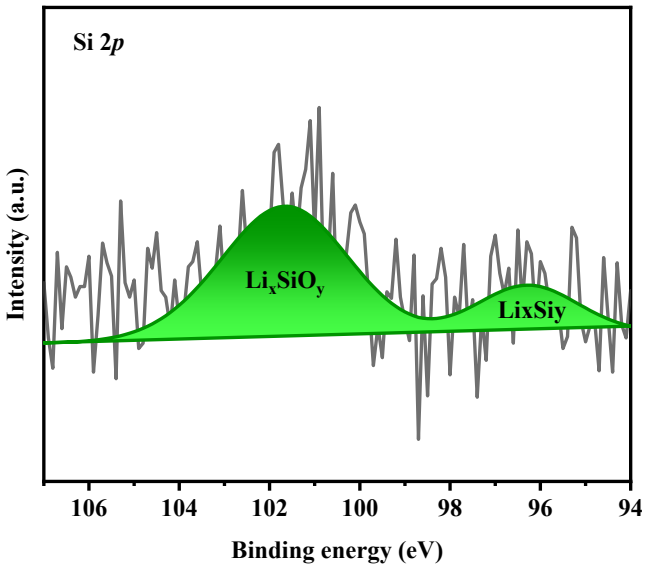

Fig. S12 The Si 2*p* spectrums of the surface of cycled ERS@Li electrode from ERS@Li||LCO pouch cell.

Compared with the Si 2*p* spectrums on initial surface of ERS@Li (Fig. S2, ESI†), after cycling, the Si 2*p* spectrums undergoes a chemical shift toward lower binding energy, indicating that more silica is reduced on the surface after cycling.

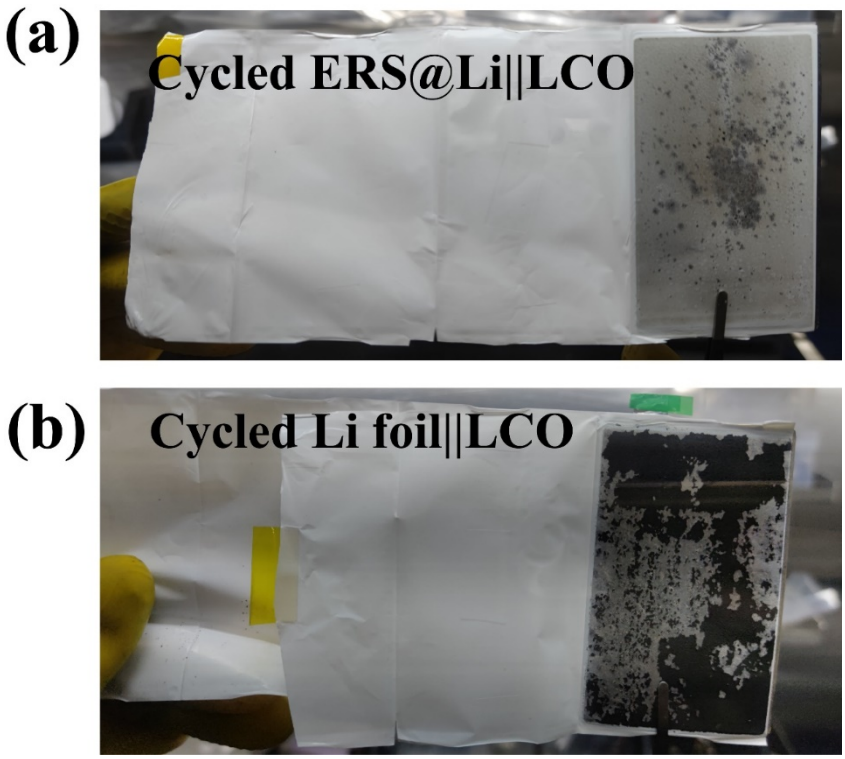

Fig. S13 The digital photos of separators from cycled **a** ERS@Li||LCO and **b** Li foil||LCO pouch cells. The Li foil||LCO pouch cell has cycled 288 times and ERS@Li||LCO pouch cell has cycled 291 times.

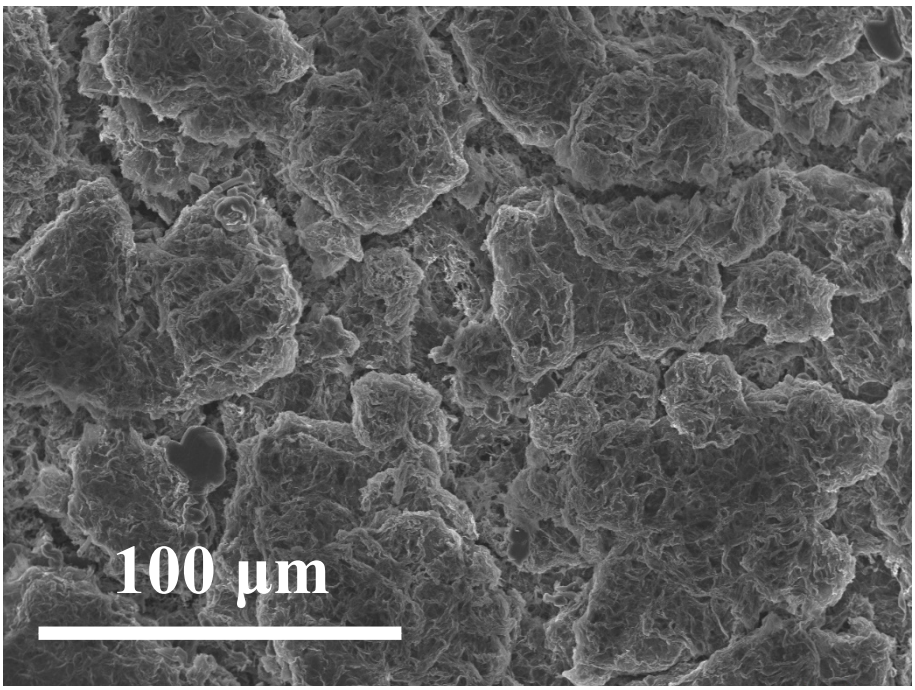

Fig. S14 The enlarged view of powdery Li on the surface of cycled ERS@Li anode in cycled ERS@Li||LCO pouch cell (discharge state at 288th cycle).

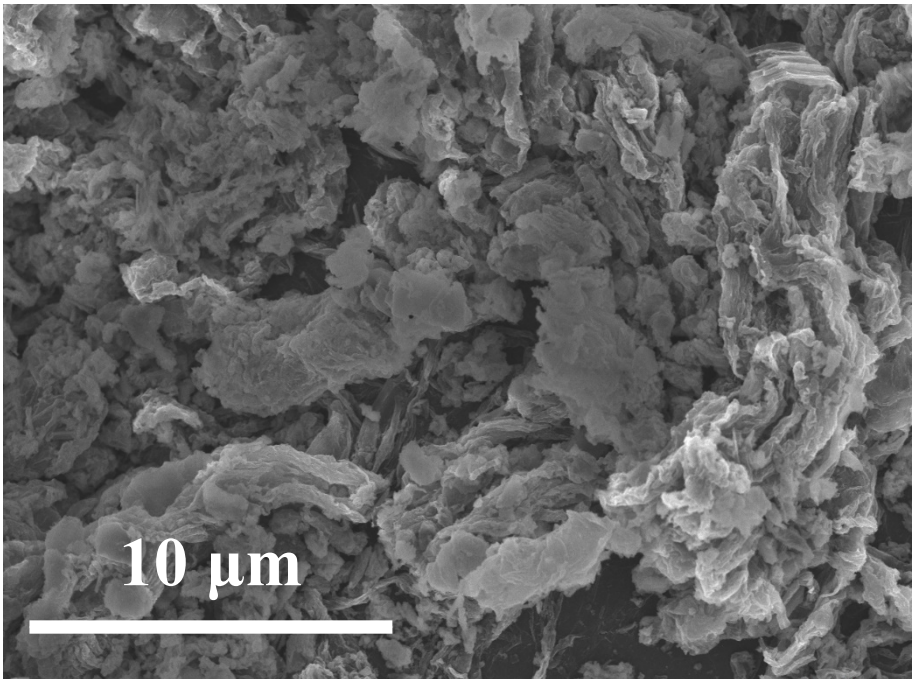

Fig. S15 The enlarged view of powdery Li on the surface of cycled Li foil anode in cycled Li foil||LCO pouch cell (discharge state at 288th cycle).

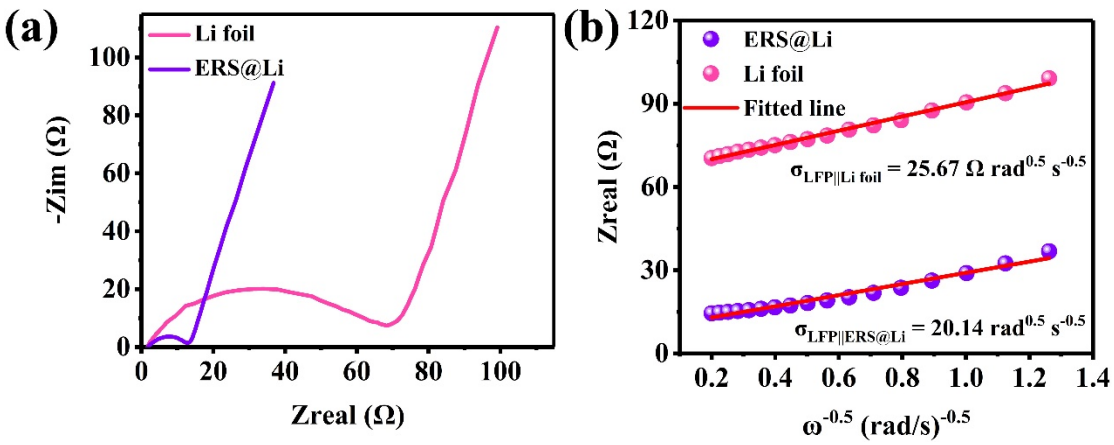

Fig. S16 a The EIS spectra of Li||LFP coin cells. **b** The relationship between Zreal and $\omega^{-0.5}$ at low-frequency region of Li||LFP cells. According to Eq. (1) and Eq. (2), the DLi of Li foil||LFP is 4.36×10^{-11} cm^2/s, and that of ERS@Li||LFP is 7.08×10^{-11} cm^2/s, which exhibits the entire reconstructed surface of Li foil can enhance the migration of Li^+.

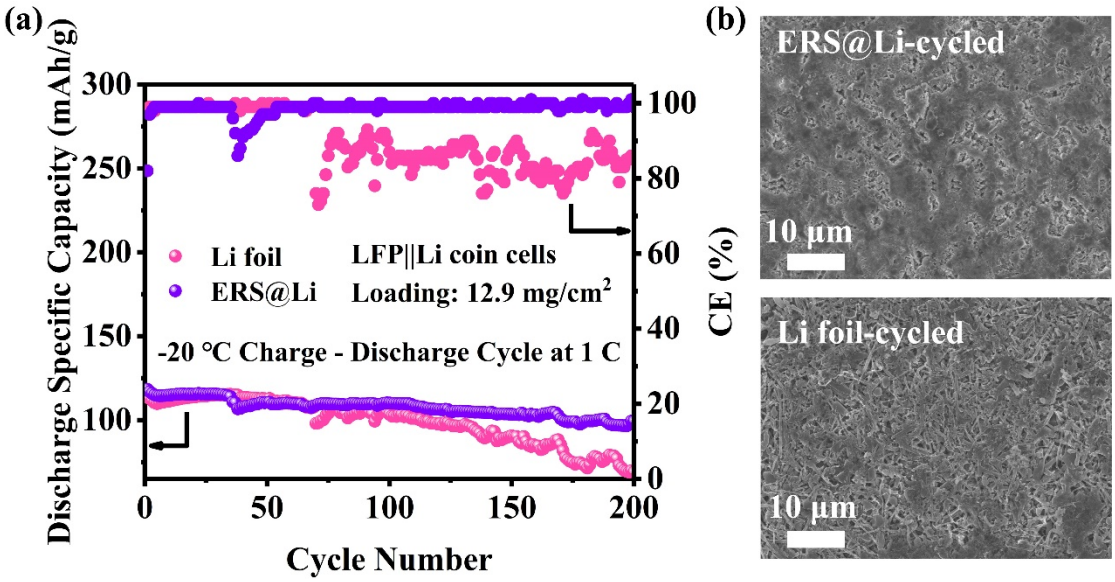

Fig. S17 a Cycling performance and **b** SEM images of cycled Li anodes of Li||LFP coin cells at -20 ℃. 1 C for Li||LFP coin cells is 170 mA/g.

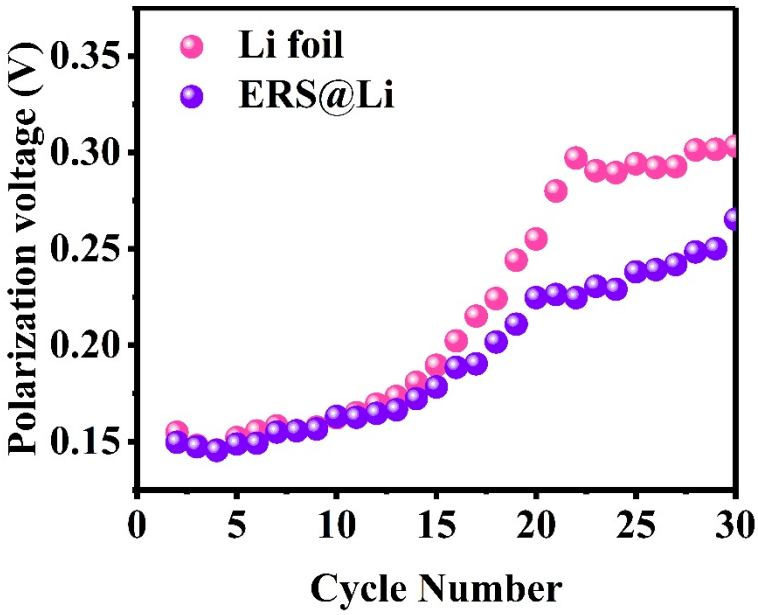

Fig. S18 The corresponding cyclic polarization voltage for **Fig. 7i**.

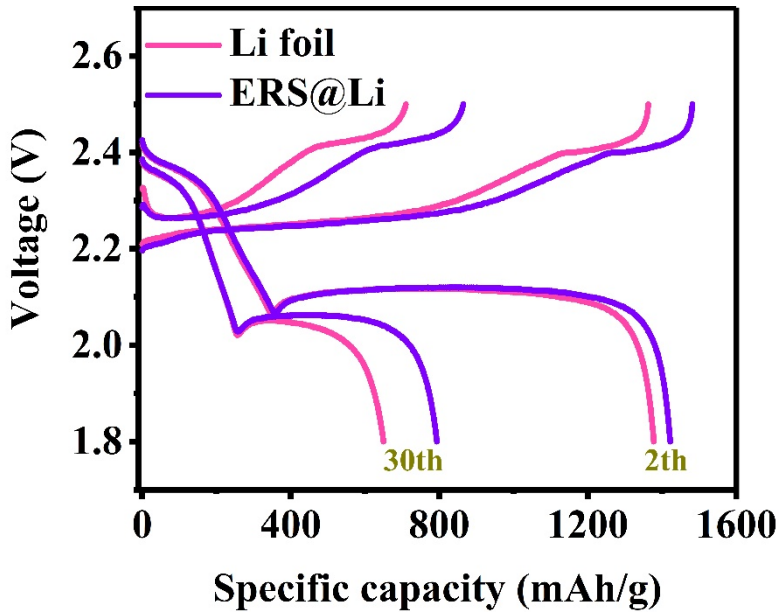

Fig. S19 Room temperature charge-charge curves at 2st cycle and 30th cycle of Li||S pouch cells with 450 Wh/Kg level.

Table S1. Detailed parameters of 0.53 Ah Li||LCO pouch cells.

Parameters	Unit	Value (Cell with ERS@Li anode)	Value (Cell with Li foil anode)
LCO content	%	98	98
Carbon content	%	1	1
Binder content	%	1	1
Electrolyte/capacity ratio	$g_{eletrolyte/capacity}$	3.0	3.0
Number of double-sided coated cathodes	\	3	3
LCO loading (single side)	mg/cm^2	17.47	17.47
Separator	Type	15 μm-thin PE	15 μm-thin PE
Size of anode	mm	50×80×0.12	50×80×0.12
Size of cathode	mm	47×77	47×77
Total mass	g	10.9	10.50
Energy density	Wh/Kg	191.93 (0.1 C)	200.29 (0.1 C)

Table S2. Comparison of performances of ERS@Li||LCO pouch cell with other literature.

pouch cell	Anode	Voltage window (V)	Capacity (Ah)	E/C ratio (g/Ah)	Cycling performance (discharge retention (cycles at charge/discharge))	References
Li||LCO	ERS@Li	4.2-3	0.53	3.0	93% (500 cycles at 0.3C/0.5C)	This work
Li||NCM83	Li foil	4.4-2.8	6.00	1.2	82% (150 cycles at 0.1C/0.5C)	[11]
Li||NCM622	Li/Cu composite foil	4.4-2.7	2.00	2.6	81% (400 cycles at 0.1C/0.3C)	[12]
Li||NCM622	Li/Cu composite foil	4.4-2.7	1.00	/	86% (200 cycles at 0.1C/0.3C)	[13]
Li||NCM811	Li/Cu composite foil	4.3-3.0	2.50	3.0	91% (50 cycles at 0.2C/0.2C)	[14]
Li||NCM811	Electrolyte engineer	3.0-4.3	5.30	2.1	92% (130 cycles at 0.1C/0.2C)	[15]
Li||LFP	LLZTO	2.5-3.8	/	/	88% (90 cycles at	[16]

composite	0.1C/0.1C)
separator	

Table S3. The detail parameters of 1.6 Ah Li||S pouch cells

Parameters	Unit	Value (Cell with ERS@Li anode)	Value (Cell with Li foil anode)
Sulfur Content	%	82	82
Carbon content	%	13	13
Binder content	%	5	5
Electrolyte/sulfur ratio	$g_{eletrolyte/sulfur}$	3.2	3.2
Number of double-sided coated cathodes	\	4	4
Weight of the sulfur	g	1.74	1.76
Sulfur loading	mg/cm^2	5.80	5.87
Size of anode	mm	80×280×0.16	80×280×0.16
Size of cathode	mm	75×50	75×50
N/P ratio at 1st	\	3.11	3.13
Total mass	g	14.78	14.76
Energy density	Wh/Kg	242.39	241.24

Table S4. Comparison of performances of ERS@Li||S pouch cell with other literature.

Capacity of pouch cell (Ah)	S loading (mg/cm^2)	Energy density (Wh/Kg)	Calculation method of energy density	E/S ratio (μL/mg)	Cycling performance	Reference
1.6	5.8	242.4	The total pouch cell	~ 3.2	96% (49 cycles at 0.1C/0.2C)	This work
6.4	4.3	466.7	The total pouch cell	~ 3.2	57% (30 cycles at 0.2C/0.2C)	This work
0.4	3.7	206	Excluding outer package	6.0	≈88% at 40^{th}	[17]
2.0	5.0	315	The total pouch cell	~ 3.2	80% (50 cycles at 0.1C/0.1C)	[18]
0.4	6.0	325	Excluding outer package	3.0	91.5% (60 cycles at 231/231 mA/g)	[19]
0.18	5.0	118	Excluding outer package	7.0	82% (50 cycles at 0.14C/0.14C)	[20]
1.0	6.5	/	/	2.5	~ 94% at 10^{th}	[21]
1.5	4.9	301	Indeterminacy	4.0	92% (30 cycles at 0.05C/0.05C)	[22]
2.0	6.0	313	The total pouch cell	2.5	~ 30% (22 cycles at 0.05C/0.05C)	[23]

4.0	7.3	451	The total pouch cell	~ 3.0	18% (19 cycles at 0.025C/0.025C)	[24]
2.3	7.2	319	The total pouch cell	~3.5	94% (20 cycles at 0.05C/0.05C)	[25]
1.6	6.1	300	The total pouch cell	3.0	81% (23 cycles at 0.025C/0.025C)	[26]
5.84	7.4	695	The total pouch cell	~1.7	24% (4 cycles at 5/5 mA/g)	[27]

References

1. K. Long, S. Huang, H. Wang, Z. Jin, A. Wang, Z. Wang, P. Qing, Z. Liu, L. Chen, L. Mei and W. Wang, *Energy Storage Materials*, 2023, **58**, 142-154.
2. G. Kresse and J. Furthmüller, *Physical Review B*, 1996, **54**, 11169-11186.
3. G. Kresse and J. Furthmüller, *Computational Materials Science*, 1996, **6**, 15-50.
4. J. P. Perdew, K. Burke and M. Ernzerhof, *Physical Review Letters*, 1996, **77**, 3865-3868.
5. J. P. Perdew, M. Ernzerhof and K. Burke, *The Journal of Chemical Physics*, 1996, **105**, 9982-9985.
6. S. Grimme, *Journal of Computational Chemistry*, 2006, **27**, 1787-1799.
7. M. Frisch, G. Trucks, H. B. Schlegel, G. Scuseria, M. Robb, J. Cheeseman, G. Scalmani, V. Barone, G. Petersson and H. Nakatsuji, *Journal*, 2016.
8. Y.-L. Wang, F. U. Shah, S. Glavatskih, O. N. Antzutkin and A. Laaksonen, *The Journal of Physical Chemistry B*, 2014, **118**, 8711-8723.
9. M. J. Abraham, T. Murtola, R. Schulz, S. Páll, J. C. Smith, B. Hess and E. Lindahl, *SoftwareX*, 2015, **1**, 19-25.
10. Y.-L. Wang, M. Golets, B. Li, S. Sarman and A. Laaksonen, *ACS Applied Materials & Interfaces*, 2017, **9**, 4976-4987.
11. H. Su, Z. Chen, M. Li, P. Bai, Y. Li, X. Ji, Z. Liu, J. Sun, J. Ding, M. Yang, X. Yao, C. Mao and Y. Xu, *Adv Mater*, 2023, DOI: 10.1002/adma.202301171, e2301171.
12. C. Niu, D. Liu, J. A. Lochala, C. S. Anderson, X. Cao, M. E. Gross, W. Xu, J.-G. Zhang, M. S. Whittingham, J. Xiao and J. Liu, *Nature Energy*, 2021, **6**, 723-732.
13. C. Niu, H. Lee, S. Chen, Q. Li, J. Du, W. Xu, J.-G. Zhang, M. S. Whittingham, J. Xiao and J. Liu, *Nature Energy*, 2019, **4**, 551-559.
14. K. Huang, S. Bi, B. Kurt, C. Xu, L. Wu, Z. Li, G. Feng and X. Zhang, *Angew Chem Int Ed Engl*, 2021, **60**, 19232-19240.
15. Q.-K. Zhang, X.-Q. Zhang, J. Wan, N. Yao, T.-L. Song, J. Xie, L.-P. Hou, M.-Y. Zhou, X. Chen, B.-Q. Li, R. Wen, H.-J. Peng, Q. Zhang and J.-Q. Huang, *Nature Energy*, 2023, DOI: 10.1038/s41560-023-01275-y.
16. C. Z. Zhao, P. Y. Chen, R. Zhang, X. Chen, B. Q. Li, X. Q. Zhang, X. B. Cheng and Q. Zhang, *Sci Adv*, 2018, **4**, eaat3446.
17. Y. Huang, M. Shaibani, T. D. Gamot, M. Wang, P. Jovanovic, M. C. Dilusha Cooray, M. S. Mirshekarloo, R. J. Mulder, N. V. Medhekar, M. R. Hill and M. Majumder, *Nat Commun*, 2021, **12**, 5375.
18. Y. Guo, Z. Jin, J. Lu, Z. Wang, Z. Song, A. Wang, W. Wang and Y. Huang, *Energy & Environmental Materials*, 2022, DOI: 10.1002/eem2.12479.
19. A. Hu, W. Chen, X. Du, Y. Hu, T. Lei, H. Wang, L. Xue, Y. Li, H. Sun, Y. Yan, J. Long, C. Shu, J. Zhu, B. Li, X. Wang and J. Xiong, *Energy & Environmental Science*, 2021, **14**, 4115-4124.
20. L. Luo, J. Li, H. Yaghoobnejad Asl and A. Manthiram, *ACS Energy Letters*, 2020, **5**, 1177-1185.
21. C. Qi, Z. Li, G. Wang, H. Yuan, C. Chen, J. Jin and Z. Wen, *Adv. Energy Mater.*, 2021, **11**, 2102024.
22. M. Zhao, X. Chen, X. Y. Li, B. Q. Li and J. Q. Huang, *Adv Mater*, 2021, **33**, e2007298.
23. L. Shi, S.-M. Bak, Z. Shadike, C. Wang, C. Niu, P. Northrup, H. Lee, A. Y. Baranovskiy, C. S. Anderson, J. Qin, S. Feng, X. Ren, D. Liu, X.-Q. Yang, F. Gao, D. Lu, J. Xiao and J. Liu, *Energy & Environmental Science*, 2020, **13**, 3620-3632.

24. Z.-X. Chen, L.-P. Hou, C.-X. Bi, Q. Cheng, X.-Q. Zhang, B.-Q. Li and J.-Q. Huang, *Energy Storage Materials*, 2022, **53**, 315-321.
25. L. P. Hou, N. Yao, J. Xie, P. Shi, S. Y. Sun, C. B. Jin, C. M. Chen, Q. B. Liu, B. Q. Li, X. Q. Zhang and Q. Zhang, *Angew Chem Int Ed Engl*, 2022, **61**, e202201406.
26. X. Q. Zhang, Q. Jin, Y. L. Nan, L. P. Hou, B. Q. Li, X. Chen, Z. H. Jin, X. T. Zhang, J. Q. Huang and Q. Zhang, *Angew Chem Int Ed Engl*, 2021, **60**, 15503-15509.
27. Q. Cheng, Z.-X. Chen, X.-Y. Li, L.-P. Hou, C.-X. Bi, X.-Q. Zhang, J.-Q. Huang and B.-Q. Li, *Journal of Energy Chemistry*, 2022, DOI: 10.1016/j.jechem.2022.09.029.